Experimental study of some properties of the strong and weak force networks in a jammed granular medium

Antoine Seguin

Noname manuscript No.
(will be inserted by the editor)

Experimental study of some properties of the strong and weak force networks in a jammed granular medium

A. Seguin

Received: date / Accepted: date

Abstract We are experimentally investigating the force network of a monolayer of grains through the jamming transition. Once the packing has been compressed beyond the volume fraction of jamming ϕ_J, we use particle tracking and photoelastic techniques to determine the network of forces in the grains. We experimentally quantify the pressure inside each grain and highlight the two networks of forces existing in jammed granular materials: the load bearing network (force chains strong network) and the dissipative network (weak network). For the strong network, we study the statistical properties of the stress state of the grains and in particular the exponential tails of the probability density function of pressure and shear stress. As the distance to jamming increases, the probability density function of local shear in the system evolves and tends to look like a normal distribution while the probability density function of pressure does not evolve. For the weak network, we study the contact cycles in the granular packing. By calculating their numbers, we determine some statistical properties of these cycles. The number of cycles of order $n = 3$ which carries the dissipative network increases linearly with the number of contacts.

Keywords Granular material · Jamming

PACS 45.70.-n 83.80.Fg

1 Introduction

Understanding the structural properties of dense divided materials, such as granular materials, remains an important and technical challenge. The structuring of the elements is at the origin of the macroscopic mechanical properties of the material. Therefore, mastering this structure during the implementation of the material is a key step for its application. Thus, to prevent a structure to collapse under a set of mechanical stresses, it is necessary that these stresses be distributed purposedly within the packing. The creation of areas of stress concentration in the weak points of the structure can spread and lead to its ruin. More generally, a granular packing consisting of polydispersed grains, characterized by a volume fraction ϕ, must have a minimum volume fraction to exhibit a certain rigidity. This particular volume fraction, called the jamming volume fraction ϕ_J, is at the onset of the appearance of the mechanical properties of the packing [1–5]. Beyond this packing fraction, the granular material no longer behaves like a glass or liquid but like a rigid deformable solid capable of transferring forces. Over the past decades and the pioneering work on forces transiting through a packing of grains [6–8], it is well established that there are mainly two force sub-networks in a granular packing. The first of these sub-networks is the load bearing network, corresponding to percolation and to the most important existing forces in the packing [9,10]. This so called strong network is characterized by the presence of force chains that pass through the packing to hang on to the walls. It has been the subject of numerous studies [9,10]. The second of these sub-networks is the so-called weak network, that is made up of the weakest and most numerous forces. The weak network contains grains subjected to forces lower than the average force in the packing. These grains have the particularity of representing more than half of the grains involved in packing [8,11]. This network, also known as the dissipative network, is characterized by contact cy-

A. Seguin
Université Paris-Saclay, CNRS, FAST, 91405, Orsay, France
SPEC, CEA, CNRS, Université Paris-Saclay, CEA Saclay 91191 Gif-sur-Yvette Cedex, France
E-mail: antoine.seguin@universite-paris-saclay.fr

cles of different lengths between the grains. These cycles mainly include forces that are not in the force chains [12–14]. The force network topology has been the subject of several studies that define parameters to characterize the geometric features of this structure [15,16]. The distribution of force level statistics and modelling of these statistics remain challenging [8,17–21] and has been studied in several static configurations with different geometries [22–26]. The study of the architecture of force chains is based on the difficulty of defining a topological criterion to characterize the statistics and the evolution of this architecture with the level of pressure in the material [27,28].

In this paper, we mainly focus on networks of forces in a vibrated granular packing. In order to simplify this approach, we use a monolayer of frictionnal grains that are compressed under vibrations. We then obtain a vibrated jammed granular medium. Particle tracking and photoelasticity techniques allow us to build the contact networks of the packing thus created and to determine the network of cycles in the packing. We measure the stress state (pressure and shear stress) in each grain. The pressure fluctuations in each grain related to vibration allow us to improve the measurement statistics. We study the statistical properties of this state of grain stress and in particular the exponential tails of pressure and shear stress distributions characterizing the strong network. Finally, we study the structure of the dissipative network by analyzing the different types of cycles and their numbers when the volume fraction ϕ varies on either side of the jamming transition ϕ_J.

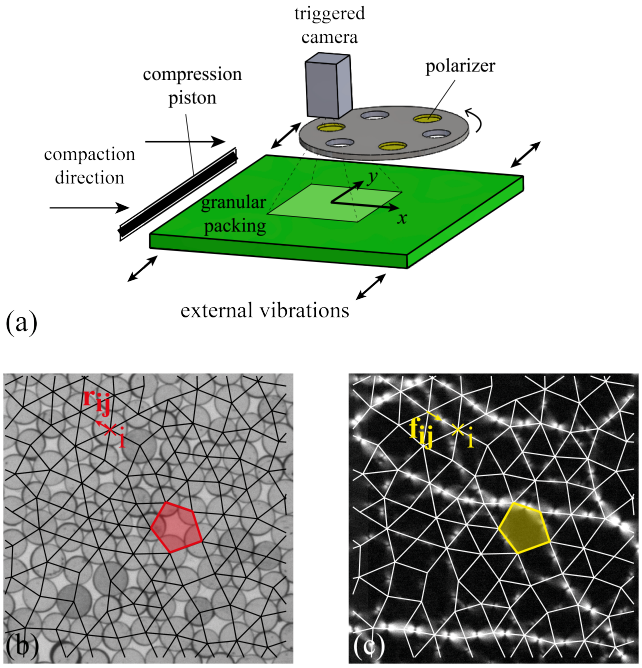

Fig. 1 Sketch of the experimental setup (a): the dark green square represents the size of the granular stack. The light green square represents the position and size of the image containing the grains under study taken by the camera located above equipped with a rotating wheel allowing to alternate polarizer and direct image. The direction of compaction is perpendicular to the direction of the external vibrations. Close-up of typical photos obtained with the experimental device for direct visualization (b) and visualization through cross-polarizers (c) at the same time for a volume fraction $\phi = 0.8262$. The contact network was calculated and then added to the photos as a mesh. We find here a i grain in contact with a j grain on the direct image by $\boldsymbol{r}_{ij}$. On the photoelastic image, we determine the force transmitted by the grain j to the grain i by $\boldsymbol{f}_{ij}$. The same five-grain cycle was highlighted in both images.

2 Experimental setup and method

We use an experimental design adapted from several previous studies [5,29–31]. Figure 1a shows a sketch of the experimental setup. This consists of an assembly of $N \simeq 8 \times 10^3$ small discs of thickness h=3,2 mm arranged between two horizontal glass plates spaced 5 mm apart and surrounded by four perpendicular side walls defining a rectangular space. This rectangular frame is not in contact with the lower glass plate on which the grains are standing. One of these walls is movable and connected to a piston that can compress the packing. These small discs are made of polyurethane (PSM4), a material with photo-elastic properties, and with diameters of 4 and 5 mm to avoid possible crystallization effects [32]. We define $d = 4$ mm. Their numbers are selected so that they occupy the same areas in the packing. This layer of grains is vibrated at a frequency of $f_0 = 10$ Hz thanks to a crankshaft-rod device (not shown in fig. 1a) linked to the bottom glass plate which allows an alternating translation motion. The knowledge of the number of grains in the packing and the position of the compression piston gives us precisely the average volume fraction ϕ of the packing. A camera located above the grain layer allows direct images of the grain location and photoelastic images showing the network of forces existing in the packing. The image taken by the camera is only a part of the frame (in its bulk). It represents approximately one sixth of the total surface area of the grains (Fig 1a). This image contains about 1500 grains. Image acquisition is synchronized with the vibration frequency. The figure 1b and 1b show a close-up of the two types of images obtained by the camera, containing about 100 grains. The direct image makes it possible to evaluate the positions of the grains over the periods and to track them. The photoelastic image coupled with the grain location information provide us a measurement of the force network throughout the pack-

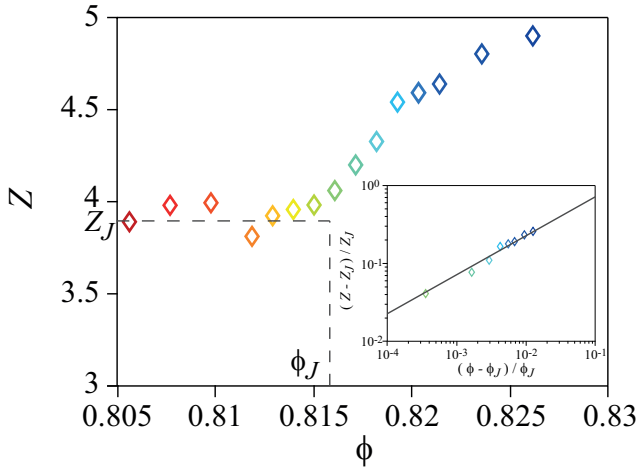

Fig. 2 Average contact number Z per grain as a function of the packing fraction ϕ. The jamming transition characterized by $\phi_J = 0.8158$ and $Z_J = 3.9$. Inset: Relative variation in the number of contacts $(Z-Z_J)/Z_J$ as a function of the relative variation in the volume fraction $(\phi-\phi_J)/\phi_J$. The solid line is a power law fit $(Z - Z_J)/Z_J = A\left((\phi - \phi_J)/\phi_J\right)^{0.5}$ with $A = 2.3 \pm 0.1$

ing [29].

In order to study the force network in the packing, it is chosen to work in decompression. The dynamics being reversible and stationary on experimental time scales during decompression phases, the packing structure remains frozen [33]. It is therefore necessary to prepare this frozen structure by a compaction protocol. Thus, the granular medium is compacted to a volume fraction beyond that of the jamming transition ϕ_J. The compaction protocol is done under vibration (at 10 Hz) and is derived from [29]. In order to have a homogeneous packing (without significant local packing fraction variation), the higher the packing fraction, the longer the medium must be vibrated [34,35]. Thus, compaction is achieved by small displacements of the compaction piston (1 or 2 mm, thus causing changes in overall packing fraction of the order of 3×10^{-4}) and the vibration time for the corresponding packing fraction increases exponentially. Once the packing is prepared, we record pairs of images (direct and photoelastic) at a volume fraction ϕ. It should be noted that all data were obtained according step by step to decreasing values of ϕ.

The correlation of successive "direct" images gives us access to the displacement field according to an Eulerian grid (x,y) of steps $dx = dy = d/10 = 0.4$ mm where x and y are the directions respectively parallel and perpendicular to the movement of the compression piston and where $d = 4$ mm represents the diameter of the small grains in the packing (Fig. 1a). The Delaunay triangulation and Voronoi tesselation are extracted from the structure and describe the neighbourhood network of each disk, thus defining the contact network [5, 29,30,36,37]. From the knowledge of the contacts and polarized images, the normal and tangential forces at the contact are then calculated by integrating the gradient of light intensity over the four areas defined by two adjoining Delaunay triangles [29]. Thus for a given grain i in contact with several grains j, the associated stress tensor can be built knowing the contact forces $\boldsymbol{f}_{ij}$ according to the definition [36,37]

$$\boldsymbol{\sigma}_i = \frac{4}{\pi {d_i}^2} \sum_{i \neq j} \boldsymbol{r}_{ij} \otimes \boldsymbol{f}_{ij} \qquad (1)$$

where d_i is the grain diameter (4 or 5 mm) and $\boldsymbol{r}_{ij}$ is the standard vector radius $d_i/2$ directed from the center of the grain i to the center of the grain j (Fig. 1). This tensor is then decomposed into a spherical and deviatoric part. We thus extract the first invariant related to the spherical part which is the pressure p_i and the second invariant related to the deviatoric part which shear stress τ_i associated with the grain i. These powerful tools have already been used in several recent numerical studies [38,39] and experimental studies [5,30]. These tools describe the stress state of the microscopic divided medium (such as granular materials) into a macroscopic effective continuous medium.

Figure 2 presents the scope of the experiments performed on both sides of the critical jamming volume fraction ϕ_J. This figure shows the evolution of Z, the average number of contacts per grain, as a function of the overall volume fraction ϕ. Z value is obtained as the arithmetic average of the contact number of each grain at all times measured during the vibration cycles. We observe that Z is constant over ϕ for lower values of ϕ and we observe that Z increases in a non-linear way with ϕ for large ϕ values. The intersection of these two regimes defines the critical volume fraction of jamming ϕ_J. In these experiments, ϕ_J is estimated at $\phi_J = 0.8158$ and Z_J is estimated at $Z_J = 3.9$. It should be noted that this value of Z_J is in line with the expected results for friction grains in [4] as $Z_J < 4$. The inset of figure 2 shows the evolution of the relative number of contacts $(Z - Z_J)/Z_J$ with the distance to criticality $(\phi - \phi_J)/\phi_J$. We observe that this behavior has already been observed experimentally, numerically, theoretically where $(Z - Z_J)/Z_J \sim \left((\phi - \phi_J)/\phi_J\right)^{\gamma}$ where γ is an exponent near 0.5 [4].

Figure 3 shows the evolution of the normalized mean pressure P_0/P_J of the packing as a function of the overall volume fraction ϕ. The pressure P_0 is obtained by averaging the pressures p_i of each grain for all times measured during the vibration cycles. For $\phi < \phi_J$, the average pressure P_0 is rather constant around a value P_J. For $\phi > \phi_J$, the pressure P_0 increases. The inset of

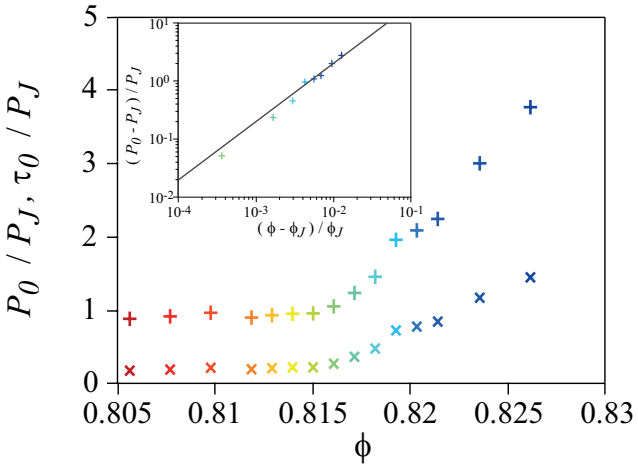

Fig. 3 Average relative pressure P_0/P_J (+) per grain and average relative shear τ_0/P_J (×) as a function of the packing fraction ϕ. Inset: Relative pressure variation $(P_0 - P_J)/P_J$ as a function of the relative variation of the volume fraction $(\phi - \phi_J)/\phi_J$. The solid line is a linear fit $(P_0 - P_J)/P_J = B(\phi - \phi_J)/\phi_J$ with $B = 208 \pm 8$

figure 3 shows the evolution of the relative pressure increase $(P_0 - P_J)/P_J$ with the criticality gap $(\phi - \phi_J)/\phi_J$. We observe that this behavior is in good agreement with previous results where $(P_0 - P_J)/P_J \sim ((\phi - \phi_J)/\phi_J)^\beta$ where β is an exponent near 1 [4]. Figure 3 also shows the evolution of the normalized average shear stress τ_0/P_J (for $\phi < \phi_J$, we call this value τ_J). We can see that the shear stress τ_J is not zero, which shows the presence of stress anisotropy in the system. The magnitude of this anisotropy is relatively small since for all measurements $\tau_0/P_J \simeq 0.1$. This anisotropy is due to the compaction protocol: the direction of the compression is perpendicular to the direction of the vibration [5].

In order to study the dissipative contact network in the packing, it is also necessary to build the contact cycles in the packing [22]. A cycle is a closed path or a nonintersecting walk of at least three grains, with no repeated grains other than its initial and final grain [40]. Defining a cycle implies that it must not contain any internal linked subcycle or smaller cycle. Figure 1 shows the result of the calculation of the cycles from the direct images and the calculation of the photoelastic contacts. The cycles measured in this study may contain up to eight grains. The number n of grains in the cycle defines the order of the cycle. Note that n varies in the range $3 \leq n \leq 8$ in the following.

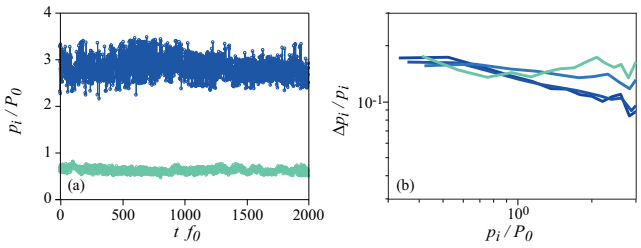

Fig. 4 (a) Evolution of the pressure in a grain as a function of the number of vibrations tf_0 carried out above ϕ_J. the number of vibrations is the product of time t with the frequency of vibration $f_0 = 10$ Hz. We present here the evolution of the pressure in a grain located in the strong network (in dark blue, with an average pressure about three times higher than P_0 for the ϕ value considered) and the evolution of the pressure in a grain located in a cycle of the weak network(in green, with an average pressure lower than P_0 for the ϕ value considered). (b) Evolution of the relative pressure fluctuation in the grains $\Delta p_i/p_i$ as a function of the average pressure p_i/P_0 of the grain.

3 Properties of the stress state fluctuations in grains

Figure 4a shows the evolution of the pressure in a grain as a function of the number of vibrations carried out in the jammed packing (the number of vibrations is the product of time t with the frequency of vibration $f_0 = 10$ Hz). It shows the evolution of two types of grain: one is arbitrarily chosen in the strong network (about three times the average pressure) and one is arbitrarily chosen in the weak network (about half the average pressure). Two different volume fractions above ϕ_J were deliberately chosen here. The pressure in a grain fluctuates over time around an average value which is the pressure p_i in the grain. The rolling average and rolling variance of p_i are constant over large time scales whether the grain is located in the strong or weak network. We can thus define the pressure fluctuation by the standard deviation of the signal, i.e. $\Delta p_i = \sqrt{< (p_i(t) - p_i)^2 >}$ where $< \cdot >$ represents the average over time of the pressure signal. We now focus on the influence of the compression level on Δp_i. Figure 4b shows the evolution of this relative fluctuation $\Delta p_i/p_i$ as a function of the average grain pressure level p_i/P_0 for different volume fractions. We observe that the fluctuation evolves in a non-trivial way: the pressure fluctuation depends both on the pressure in the grain p_i (depending on whether it is located in the strong or weak network) and on the jamming gap $\phi - \phi_J$. For the less dense packing (low values of $\phi - \phi_J$, close to jamming), the relative pressure fluctuation is constant regardless of the grain pressure level. But as the density increases (high values of $\phi - \phi_J$, far from jamming), the relative pressure fluctuation decreases in the most mechanically stressed grains (high values of p_i/P_0), i.e. those in the stong network. In fact,

it would seem that it is the absolute pressure fluctuation that is constant. In the weak network, the relative pressure variation remains constant.

We now focus on the distribution of pressure and shear stress in the system (Fig. 5). Force distribution has been extensively studied in granular packings through normal and tangential force distributions [8]. We investigate further these studies here with the quantities p_i and τ_i that are present even in the numerical case of frictionless grains. Figure 5 represents the probability density functions of p_i and τ_i for packings at different ϕ. For $\phi > \phi_J$, we can see that the distributions show an exponential tail characteristic of the forces transiting in granular materials (Fig. 5a and 5b) but also in other materials where the jamming transition exists such as emulsions [19]. One of the force distribution models comes from the q-model [17] where force distribution is a power law for the lower values of forces and present an exponential tail for the higher values of forces. The generic expression of this distribution is as follows:

$$Pdf(v) = Av^{N-1}\exp(-Nv) \quad (2)$$

where N is theoretically related to the average number of neighbors of grains, A is a numerical prefactor and v the quantity referred to [17,19]. In figure 5, equation 2 was plotted with $N = 2$ and $A = 4$. Theses values are quite close to the ones obtained numerically [8,11,41]. Above ϕ_J we see that this model reproduces well the distribution of pressure stresses in all areas (Fig. 5a). It is also important to note that there is a nonzero pressure probability at zero pressure. Unlike the distribution of pressure p_i, we also observe that the distribution of τ_i is not independent of ϕ (Fig. 5b). Indeed, when ϕ decreases, the exponential tail softens and becomes less heavy-tailed. This variation in the exponential tail at high shear value has already been reported in numerical studies [18,21,41]. To describe the behaviour of the exponential tail, we choose here to use the form $Pdf(\tau_i) \sim \exp(-N{\tau_i}^{\alpha})$ where α is an exponent characterizing the heaviness of the exponential tail with ϕ [18]. Figure 6 shows the evolution of α with ϕ. We observe that α varies from 0.6 to 2.2 according to the measurements, which tends to describe the distribution as a Gaussian distribution for the higher values of ϕ [18]. The growth of α with ϕ was found in a numerical study in the same range [21]. All this indicates that the distribution of local shear in the system tends to homogenize as the average pressure level (and also the average shear level) increases (inset of fig. 6).

For $\phi < \phi_J$, we notice that all the distributions of p_i and τ_i collapse on a master curve (Fig. 5c and 5d). For lower stress values, the probability decreases as the stress decreases and tends towards 0. The decrease for higher stress values is exponential but the decrease is less important for shear values τ_i than for pressure values p_i. Below ϕ_J, the modeling by the equation 2 is not relevant because there is no existence of a strong and weak network since the packing is not jammed. However, the model was drawn on the figure as a guideline for the eyes (Fig. 5c and 5d).

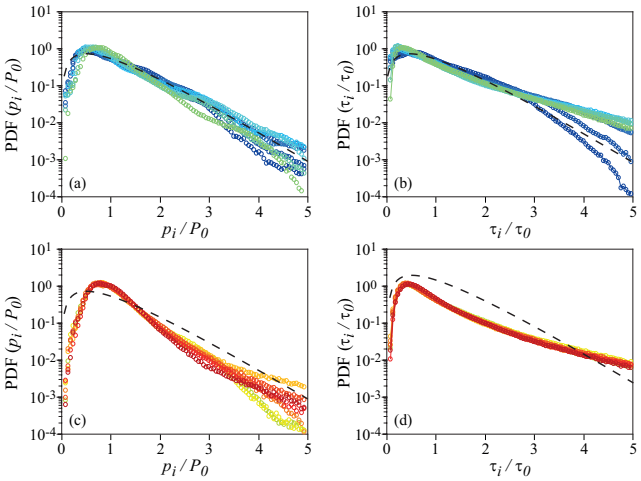

Fig. 5 Probability density function of the normalized pressure p_i/P_0 for (a) $\phi > \phi_J$ and for (b) $\phi < \phi_J$. Probability density function of normalized shear τ_i/τ_0 for (c) $\phi > \phi_J$ and for (d) $\phi < \phi_J$. The dotted curves represent the equation 2 of the form $Pdf(v) = 4v\exp(2v)$ and is used as a guide for the eyes.

4 Properties of the cycle network in the packing

One of the main elements constituting the weak network of forces are the grains that will ensure the resisting connection of forces in the main force chains. This resisting connection of the structure's efforts is done through contacts between the grains in the strong network and which redistributes the efforts on the weak network. To characterize the structure of this stress recovery, we study here the contact cycles. Contact cycles are directly related to the mechanical stability of the structure [26]. Figure 1 shows a cycle of five contacting grains in which the forces of the strong network are redistributed. In addition, in that figure, the complete network of contact between the grains has been drawn in order to reveal all the cycles: the cycles are represented here by convex polygons whose vertices are the centres of the grains in contact connected by the edges. Thus, we call the order n of a cycle the order of the characteristic polygon that constitutes it: n therefore also represents the number of grains involved in the cycle. In the following, we focus on the quantity of these cycles that build up the packing. Thus, the number of

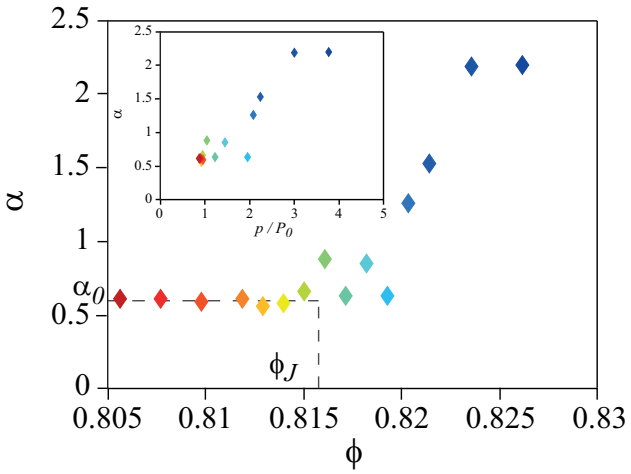

Fig. 6 Evolution of the parameter α characterizing the exponential tail of the distribution of shear as a function of the packing fraction ϕ. For $_\phi < \phi_J$, α has an average value of $\alpha_0 = 0.6 \pm 0.1$. Inset: evolution of the parameter α characterizing the exponential tail of the distribution of shear as a function of the relative pressure p/P_0.

cycles of an order n existing in the packing is noted $\mathcal{L}_n$. We notice that the figure is mainly composed of cycles of order $n = 3$ (triangles) which constitute the major structure of the weak network but the other orders are also present. Previous numerical studies have focused on cycles of order $n = 3$ [12–14]. These cycles are the main components of the weak force network. In particular, it was presented that the number of these cycles, $\mathcal{L}_3$, increased with the contact number, Z, such as $\mathcal{L}_3 \sim Z^3$ [13] or such as $\mathcal{L}_3 \sim Z$ [14].

First, we are interested in the total number of cycles, $\mathcal{L}_T$. $\mathcal{L}_T$ is the sum of all $\mathcal{L}_n$ cycles of order n (with $3 \leq n \leq 8$) such as $\mathcal{L}_T = \sum_{n=3}^{n=8} \mathcal{L}_n$. Figure 7a shows the evolution of the total number of cycles, $\mathcal{L}_T$, in the sample measured as a function of the volume fraction ϕ. For $\phi < \phi_J$, $\mathcal{L}_T$ remains roughly constant and increases with ϕ starting from $\phi > \phi_J$. Although the system is jammed, this shows that there is still a structural evolution of the packing. The strong network is characterized by long chains that run through the material from one edge to the other and remains stable even if ϕ varies. Consequently, the strong network is created at jamming. On the other hand, as soon as the volume fraction ϕ becomes smaller than ϕ_J, this network is not stable and is likely to evolve. We do not find spatially the same long chains in the material. The weak network is characterized by the cycles. We observe that these cycles evolve with ϕ when ϕ is greater than ϕ_J. In order to follow these evolutions, we study the number of cycles of order n, noted $\mathcal{L}_n$ (with $3 \leq n \leq 8$). Figure 7b shows the relative evolution of the number of cycles of order n, noted $\mathcal{L}_n/\mathcal{L}_T$ as a function of the volume fraction ϕ. For $\phi < \phi_J$, the number of cycles remains roughly constant regardless of the order of the cycle n: this value is noted n is noted Λ_n in the following. For $\phi > \phi_J$, the number of cycles of order $n = 3$ and $n = 4$ increases (which is more visible in figure 7c with a linear scale). In contrast, the number of cycles of order $n \geq 5$ decreases with ϕ, which confirms that the system breaks its high order cycles to create new ones of lower order n. It should be noted for order $n \geq 6$, cycles do not necessarily contain grains trapped inside, such as rattlers. These cycles have a rather elliptical appearance with a high aspect ratio. With the increase of ϕ from the critical volume fraction ϕ_J, cycles of large order ($n \geq 5$) are broken (and therefore create contacts in the system to ensure the recovery of effort from the large network) to promote the creation of cycles of small order ($n \leq 4$) in particular cycle of order $n = 3$. The weak network builds up through its cycles of order $n = 3$ which are more and more numerous as ϕ increases. In addition, figure 7c shows the relative variation of the small order cycles $(\mathcal{L}_n - \Lambda_n)/\Lambda_n$ ($3 \leq n \leq 5$). In the same way as in figure 2, it is possible to highlight the significant growth in the number of cycles for $\phi = \phi_J$. This singularity in the creation of cycles is a signature of the jamming transition. We observe that it is the creation of cycles of order $n = 3$ that is predominant beyond ϕ_J. Figure 7d shows the evolution of the amount of cycles of order $n = 3$ relative to the increase in the number of contacts at the jamming. We observe a linear relationship in the growth of the amount of cycles of order $n = 3$ and the increase in the number of contacts such that $(\mathcal{L}_3 - \Lambda_3)/\mathcal{L}_T \sim (Z - Z_J)/Z_J$. It is this scaling that is hidden in the evolution of the total number of cycles $\mathcal{L}_T$ with ϕ since more than 80% of the cycles constituting $\mathcal{L}_T$ are cycles of order 3 (Fig. 7b). This scaling law is quite different from the one presented numerically (in Z^3) [13] but in excellent agreement with [14]. Since the total number of cycles is mainly made up of triangles, this also leads to $\mathcal{L}_T \sim Z$ for $\phi > \phi_J$. Above jamming, when a contact link is created through an increase of ϕ, the probability for creating a new cycle of order $n = 3$ (and break a high order cycle) is constant [14].

5 Conclusion and perspectives

In this experimental study, we highlighted some statistical properties of the force network in a jammed granular packing. To do this, from a 2D packing of photoelastic discs, a jammed packing is created and the contact network between the grains is identified. In a first step, we have validated that the packing respects two usual scaling laws for jamming: the scaling between the number

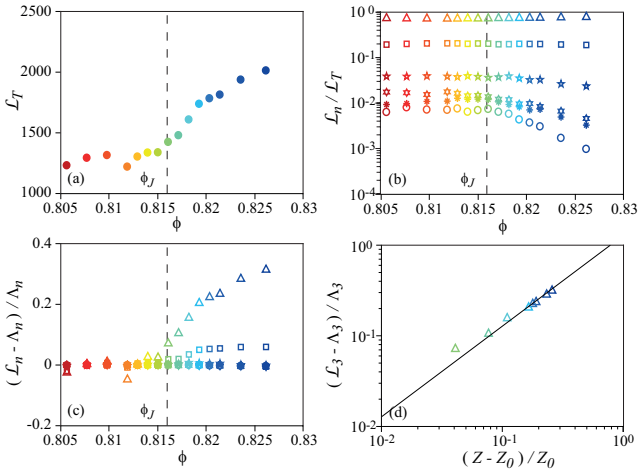

Fig. 7 (a) Total number of cycles $\mathcal{L}_T$ in the sample measured according to the packing fraction ϕ. (b) Relative number of cycles of order n $\mathcal{L}_n/\mathcal{L}_T$ depending on the packing fraction ϕ. The symbols correspond to $n = 3$ ($\triangle$), $n = 4$ ($\square$), $n = 5$ ($\star$), $n = 6$ ($\hexagram$), $n = 7$ ($*$) and $n = 8$ ($\circ$). (c) Relative number of cycles of order n $(\mathcal{L}_n - \Lambda_n)/\Lambda_n$ depending on the packing fraction. The symbols correspond to $n = 3$ ($\triangle$), $n = 4$ ($\square$), $n = 5$ ($\star$) and $n = 6$ ($\hexagram$). (d) Relative number of cycles of order n =3 $(\mathcal{L}_3 - \Lambda_3)/\Lambda_3$ depending on the relative number of contacts $(Z - Z_0)/Z_0$. The solid line is a linear fit $(\mathcal{L}_3 - \Lambda_3)/\Lambda_n = C(Z - Z_0)/Z_0$ with $C = 1.3 \pm 0.1$.

of contacts and the volume fraction $Z \propto \phi^{0.5}$ and the pressure - volume fraction relationship $P_0 \propto \phi$. The analysis of the photoelastic images shows the presence of a strong network called load bearing network and a weak network that ensures the resisting connection of the strong network to dissipate them in another network in the packing called disspative network [8]. Thus the weak network relieves the strong network.

The presence of a strong network characterized by long chains of forces crossing the entire network is analyzed in terms of the average pressure level in each grain. The statistical distributions of pressure level and shear stress show exponential tails for high pressure values. While the pressure distribution varies rather exponentially with ϕ, the shear stress distribution tends towards a Gaussian as ϕ increases.

The presence of the weak network is characterized by the presence of grain cycles linked to the strong network made of several grains. These cycles are characterized by their order n (n being the number of grains constituting the cycle). The total number of these cycles $\mathcal{L}_T$ increases with the volume fraction ϕ. However, the number of cycles of a given order n does not systematically increase with the volume fraction. It is mainly the numbers of cycles of order $n = 3$ and $n = 4$ that increase with ϕ while the number of cycles $n \geq 5$ decreases with ϕ increases. The system therefore creates contacts by destroying cycles of large order n and creating cycles of small order n and mainly cycles of order $n = 3$. The increase in the total number of cycles $\mathcal{L}_T$ is mainly due to the creation of cycles of order $n = 3$. In addition, the increase of cycles of order $n = 3$ with the number of contacts follows a linear scaling law $\mathcal{L}_3 \propto Z$. This experimental study presents statistical information on pressure levels, shear stress and cycle organization in jammed granular packing. These quantities are relevant elements in order to understand the macroscopic stress response of granular materials, which remains an unresolved problem. The ultimate goal of all these studies would be to link the structure of the force chains and network to the properties of the material for a better understanding of its topology and thus create and control one's own material.

Acknowledgements The author is grateful to V. Padilla and C. Wiertel-Gasquet for the development of the experimental setup and to L. Talon for fruitful discussion.

Conflict of interest

The authors declare that they have no conflict of interest.

References

1. A.J. Liu, S.R. Nagel, Nature **396**(6706), 21 (1998)
2. C.S. O'Hern, S.A. Langer, A.J. Liu, S.R. Nagel, Physical Review Letters **88**(7), 075507 (2002)
3. C.S. O'Hern, L.E. Silbert, A.J. Liu, S.R. Nagel, Physical Review E **68**(1), 011306 (2003)
4. M. van Hecke, J. Phys. Condens. Matter **22**(3), 033101 (2010)
5. C. Coulais, A. Seguin, O. Dauchot, Phys. Rev. Lett. **113**, 198001 (2014). DOI 10.1103/PhysRevLett.113.198001
6. T. Travers, D. Bideau, A. Gervois, J. Troadec, J. Messager, Journal of physics A: mathematical and general **19**(16), L1033 (1986)
7. C.h. Liu, S.R. Nagel, D. Schecter, S. Coppersmith, S. Majumdar, O. Narayan, T. Witten, Science **269**(5223), 513 (1995)
8. F. Radjai, M. Jean, J.J. Moreau, S. Roux, Physical review letters **77**(2), 274 (1996)
9. S. Ostojic, E. Somfai, B. Nienhuis, Nature **439**(7078), 828 (2006)
10. S.N. Pathak, V. Esposito, A. Coniglio, M.P. Ciamarra, Physical Review E **96**(4), 042901 (2017)
11. F. Radjai, S. Roux, J.J. Moreau, Chaos: An Interdisciplinary Journal of Nonlinear Science **9**(3), 544 (1999)
12. R. Arevalo, I. Zuriguel, D. Maza, International Journal of Bifurcation and Chaos **19**(02), 695 (2009)
13. R. Arévalo, I. Zuriguel, S.A. Trevijano, D. Maza, International Journal of Bifurcation and Chaos **20**(03), 897 (2010)
14. R. Arévalo, I. Zuriguel, D. Maza, Physical Review E **81**(4), 041302 (2010)
15. L. Kondic, A. Goullet, C. O'Hern, M. Kramar, K. Mischaikow, R. Behringer, EPL (Europhysics Letters) **97**(5), 54001 (2012)

16. M. Kramar, A. Goullet, L. Kondic, K. Mischaikow, Physical Review E **87**(4), 042207 (2013)
17. S. Coppersmith, C.h. Liu, S. Majumdar, O. Narayan, T. Witten, Physical Review E **53**(5), 4673 (1996)
18. A.R. van Eerd, W.G. Ellenbroek, M. van Hecke, J.H. Snoeijer, T.J. Vlugt, Physical Review E **75**(6), 060302 (2007)
19. K.W. Desmond, P.J. Young, D. Chen, E.R. Weeks, Soft Matter **9**(12), 3424 (2013)
20. D.S. Bassett, E.T. Owens, M.A. Porter, M.L. Manning, K.E. Daniels, Soft Matter **11**(14), 2731 (2015)
21. X. Deng, R.N. Davé, Granular Matter **19**(2), 27 (2017)
22. A. Tordesillas, D.M. Walker, Q. Lin, Physical Review E **81**(1), 011302 (2010)
23. D.M. Walker, A. Tordesillas, International Journal of Solids and Structures **47**(5), 624 (2010)
24. D.S. Bassett, E.T. Owens, K.E. Daniels, M.A. Porter, Physical Review E **86**(4), 041306 (2012)
25. R. Arévalo, L.A. Pugnaloni, I. Zuriguel, D. Maza, Physical Review E **87**(2), 022203 (2013)
26. A.G. Smart, J.M. Ottino, Physical Review E **77**(4), 041307 (2008)
27. C. Giusti, L. Papadopoulos, E.T. Owens, K.E. Daniels, D.S. Bassett, Physical Review E **94**(3), 032909 (2016)
28. L. Papadopoulos, J.G. Puckett, K.E. Daniels, D.S. Bassett, Physical Review E **94**(3), 032908 (2016)
29. C. Coulais, R.P. Behringer, O. Dauchot, Soft Matter **10**, 1519 (2014). DOI 10.1039/C3SM51231B
30. A. Seguin, C. Coulais, F. Martinez, Y. Bertho, P. Gondret, Physical Review E **93**(1), 012904 (2016)
31. A. Seguin, P. Gondret, Physical Review E **96**(3), 032905 (2017)
32. O. Pouliquen, M. Nicolas, P. Weidman, Physical Review Letters **79**(19), 3640 (1997)
33. F. Lechenault, O. Dauchot, G. Biroli, J.P. Bouchaud, EPL **83**, 46003 (2008). DOI 10.1209/0295-5075/83/46003
34. J.B. Knight, C.G. Fandrich, C.N. Lau, H.M. Jaeger, S.R. Nagel, Physical review E **51**(5), 3957 (1995)
35. P. Richard, M. Nicodemi, R. Delannay, P. Ribiere, D. Bideau, Nature materials **4**(2), 121 (2005)
36. A. Drescher, G. de Josselin de Jong, J. Mech. Phys. Solids **20**, 337 (1972)
37. D. Bi, J. Zhang, B. Chakraborty, R.P. Behringer, Nature **480**, 355 (2011)
38. P.P. Cortet, D. Bonamy, F. Daviaud, O. Dauchot, B. Dubrulle, M. Renouf, EPL (Europhysics Letters) **88**(1), 14001 (2009)
39. A. Seguin, A. Lefebvre-Lepot, S. Faure, P. Gondret, The European Physical Journal E **39**(6), 63 (2016)
40. B. Bollobás, O. Riordan, in *Handbook of large-scale random networks* (Springer, 2008), pp. 15–115
41. F. Radjai, Comptes Rendus Physique **16**(1), 3 (2015)